

NEW SILHOUETTE DISKS WITH REFLECTION NEBULAE AND OUTFLOWS IN THE ORION NEBULA AND M43¹

Nathan Smith², John Bally, Daniel Licht, and Josh Walawender

Center for Astrophysics and Space Astronomy, University of Colorado, 389 UCB, Boulder, CO 80309

ABSTRACT

We report the detection of several new circumstellar disks seen in silhouette against background nebular light in the outskirts of the Orion nebula and the neighboring H II region M43. These were detected as part of our H α survey of Orion with the Advanced Camera for Surveys on-board the *Hubble Space Telescope*. Several of the disks show bipolar reflection nebulae, microjets, or pronounced temporal variability of their central stars. The relatively large fraction of bipolar reflection nebulae or microjets in our sample may be a selection effect caused by the faint nebular background far from the Trapezium. Two disks in our sample are large and particularly noteworthy: A nearly edge-on disk, d216-0939, is located several arcminutes northwest of M43 and resembles the famous HH 30 disk/jet system in Taurus. It drives the 0.15 pc long bipolar outflow HH 667, and exhibits a remarkable asymmetric reflection nebula caused by the tilt of the flared disk. With a diameter of $\sim 2''.6$ (1200 AU), d216-0939 is as large as the giant edge-on silhouette disk d114-426 in the core of the Orion Nebula. The large disk d253-1536 is located in a binary system embedded within an externally-ionized giant proplyd in M43. The disk exhibits distortions which we attribute to tidal interactions with the companion star. The bipolar jet HH 668 emerges from the proplyd ionization front in a direction orthogonal to the disk, and can be traced to the young star embedded within it. A bow shock lies $54''$ south of this binary system along the outflow axis. Proper motions over a 1.4 yr baseline confirm that these emission knots are indeed moving away from d253-1536, with speeds as high as ~ 330 km s⁻¹ in the HH 668 microjet, and slower motion farther from the star.

Subject headings: ISM: Herbig-Haro objects — ISM: individual (M42, M43) — ISM: jets and outflows — planetary systems: protoplanetary disks — reflection nebulae — stars: formation — stars: pre-main-sequence

1. INTRODUCTION

The *Hubble Space Telescope* (*HST*) has produced remarkable images of circumstellar disks surrounding young stars. By far the largest population of known circumstellar disks is located in the Orion nebula at a distance of 460 pc (see Bally et al. 2000), where the disks have typical diameters of 50-1000 AU. O’Dell, Wen, & Hu (1993) found several disks seen in silhouette against the background nebular light, and dozens of young stellar objects surrounded by teardrop- or tadpole-shaped ionization fronts. These are protoplanetary disks seen purely in silhouette, or externally-ionized photo-ablating protoplanetary disks (“proplyds”), both

¹Based on observations made with the NASA/ESA *Hubble Space Telescope*, obtained at the Space Telescope Science Institute, which is operated by the Association of Universities for Research in Astronomy, Inc., under NASA contract NAS5-26555.

²Hubble Fellow; nathans@casa.colorado.edu

rendered visible by their location in or near an H II region (O’Dell et al. 1993, 1996; McCullough et al. 1995; Bally et al. 1998, 2000). McCaughrean & O’Dell (1996) found six additional disks seen purely in silhouette against the bright nebular emission from the Orion nebula. More detailed *HST* imaging studies of the nebular core revealed a total of 15 silhouette disks (Bally, McCaughrean, & O’Dell 2000; McCaughrean et al. 1998) and nearly 200 bright proplyds (O’Dell et al. 1993; O’Dell & Wong 1996; Bally et al. 1998, 2000). Some silhouette disks are seen embedded inside bright proplyds (Bally et al. 2000), where in some cases the disks glow in [O I] and H₂ emission (Chen et al. 1998; Störzer & Hollenbach 1998). In addition, several one-sided “microjets” are associated with proplyds (Bally et al. 2000; Reipurth & Bally 2001), indicating that the embedded stars are still surrounded by active accretion disks.

So far, only the inner portion of the Orion nebula – a region that contains about 400 of the nearly 2,000 members of the extended Trapezium cluster of low mass stars – has been completely surveyed with *HST*. However, O’Dell (2001) presented HST images of several objects outside the nebular core, demonstrating that additional young stars, disks, and jets remain to be discovered in the outer regions of the Orion nebula.

With the new Wide Field Camera of the Advanced Camera for Surveys (ACS/WFC) installed on *HST* during the 2002 servicing mission, we explored the outer Orion Nebula where radiation fields are less intense than in the nebular core. The outskirts of the Orion nebula contain young stars bathed in radiation fields that may be more typical of the environment in which most stars in the sky are born. The survey samples a large portion of the Orion Nebula Cluster. Our ACS/WFC survey also included the first comprehensive *HST* imaging of the neighboring H II region M43, several arcminutes north of the Trapezium, powered by the single B0-type star NU Ori.

The new disks are seen despite the the fainter background nebular emission far from the Trapezium. On the other hand, the faint nebular background probably makes it easier to see extended emission from bipolar reflection nebulae and microjets emerging from the silhouette disks — phenomena which are apparently less common among pure silhouette disks in the inner Orion nebula (Bally et al. 2000). After a general description of these new silhouette disks (§3), we provide more detailed investigations of two particularly interesting disks and their associated jets (§4 and §5). One additional proplyd with a bipolar jet and silhouette disk, d181-826 and HH 540, is also seen in our survey in the outer parts of the Orion nebula, but has been discussed separately (Bally et al. 2004) because of its remarkable morphology.

2. OBSERVATIONS

The new ACS/WFC observations reported here were extracted from images obtained as part of an H α survey of the Orion Nebula and M43 during *HST* Cycle 12, using the F658N filter to cover 415 square arcminutes. The narrowband F658N filter transmits both H α and [N II] λ 6583 in the nebula, although for simplicity we refer to it as an H α filter. Further details of the Cycle 12 observations and data reduction procedures are given in an earlier paper in this series (Bally et al. 2004), and are not repeated here.

In addition to these Cycle 12 observations, we obtained ACS/WFC images at four pointings during Cycle 11, using the F658N filter, the F660N filter which only transmits [N II] λ 6583, the F502N filter sampling [O III] λ 5007, and the F550M continuum filter. These Cycle 11 data, obtained on 2002 August 29 and 30, led to the discovery of the d216-0939 silhouette disk (see §4), which was not observed during Cycle 12, and for measuring proper motions in the HH 668 jet associated with d253-1536, which was observed in both Cycle 11 and 12 (see §5). The Cycle 11 observation strategy differed in minor ways from the Cycle 12 program. For each pointing in the F658N filters during Cycle 11, two exposures with a duration of 500 seconds each

were obtained with a two-point dither pattern in which the second exposure was offset from the first by $5''$ toward both the east and the south. This two-point dither pattern served to fill the gap between the two 2048×4096 pixel CCD arrays of the ACS/WFC, and in the fields which were common to both exposures served to identify cosmic ray hits. Table 1 lists the central coordinates and other parameters of the Cycle 11 ACS/WFC observations.

3. NEW SILHOUETTE DISKS

Figure 1 shows ten $H\alpha$ images of silhouette disks extracted from our ACS/WFC survey of Orion; each frame is $7'' \times 7''$. The name of each disk follows the coordinate-based naming convention of O’Dell & Wen (1994), with the prefix “d” for disk. A few objects show evidence for either bipolar “microjets” (see Reipurth & Bally 2001; Bally et al. 2000) or reflection nebulae. Since we obtained only narrowband $H\alpha$ images for most objects, spectra are needed to distinguish reflection nebulae from jets. Coordinates and basic properties of each object are summarized in Table 2, and a brief description of each disk is given below.

d053-717 (Figure 1a). A small silhouette disk with a bright central star is seen roughly $5'$ southwest of the Trapezium outside the bright Huygens region. The outer edge of the silhouette disk has a diameter of $\sim 0''.9$ (410 AU). The disk has a length-to-width ratio of roughly 5 suggesting a high inclination, but it cannot be purely edge-on since a bright central star is visible. Thus, the inclination angle is probably of order $75^\circ \pm 10^\circ$. No sign of a bright proplyd ionization front is seen.

d110-3035 (Figure 1b). This unusual object appears to be a nearly edge-on disk with a bright bipolar reflection nebula. An edge-on dark disk much like some other disks seen by *HST* (Padgett et al. 1999; Stapelfeldt et al. 2003) bisects the small nebula along P.A. $\simeq 0^\circ$. The extended portions of the disk are difficult to see against the faint background nebula, with a diameter of roughly $0''.9$ (410 AU) or more. Two emission or reflection knots are distributed nearly symmetrically on either side of the disk along an east/west axis perpendicular to the disk.

d124-132 (Figure 1c). A bright proplyd with a small disk inside is found about 1.5 north of the Trapezium. The proplyd ionization front has dimensions of $1''.2 \times 2''$, with the brightest part of the front facing the Trapezium. The disk has a diameter of $\sim 0''.5$ (230 AU) with a likely inclination angle of $\sim 75^\circ$, and shows faint emission from a bipolar reflection nebula or microjet emerging perpendicular to the major axis of the disk. This polar emission is brighter on the western side of the disk, suggesting that the western part of the polar axis is tilted toward us out of the plane of the sky. A faint protrusion in the proplyd on the western rim along the disk axis may mark the location of a shock powered by a jet.

d132-042 (Figure 1d). d132-042 has a similar size and inclination as the previous disk, d124-132, it is also embedded in a bright proplyd, and is located near to it on the sky. It has a bipolar microjet that is very faint on the northern side of the disk, but is bright and extends at least $0''.4$ to the south and intrudes into the disk on the southern side (thus, this is probably the blueshifted part of the jet). There is another bright knot along the presumed jet axis $0''.7$ south of the source, but this also appears to be the location of the surrounding proplyd ionization front.

d132-1832 (Figure 1e). Bally et al. (2000) discovered this large silhouette disk, located north of the Trapezium near the edge of the bright inner Orion Nebula. It is discussed here because our ACS/WFC $H\alpha$ image provides new information in two respects. First, the new image has higher resolution and sensitivity than earlier Wide Field Planetary Camera 2 (WFPC2) images, and shows that faint translucent material in

the outer parts of the disk is apparently getting swept-back (to the north) by radiation pressure or a large-scale wind from the Trapezium, located toward the south. Second, the previous WFPC2 image obtained in Cycle 6 (1998 Apr 4) shows a very bright central star (see the inset of Figure 1*d*), while the star has completely faded from visibility in our new ACS image. The F656N filter of WFPC2 also samples H α but is narrower than the F658N filter of ACS (i.e. the ACS filter contains more continuum light). Therefore, the central star is significantly variable, and it is unclear whether the change is caused by continuum or line emission. If the excess emission in the earlier WFPC2 image in 1998 is due to an H α flare, then this emission line’s intrinsic luminosity in the central source decreased by at least $\sim 4 \times 10^{27}$ ergs s $^{-1}$ over a period of only 5 years.

d141-1952 (Figure 1*f*). The dark region between M42 and M43 harbors a star surrounded by a small disk seen in silhouette against the background nebular light. The disk has a major-axis diameter of roughly 0.7'' and a minor-axis diameter of about 0.6'' (320 \times 275 AU), implying that its polar axis is tilted about 55-60° out of the plane of the sky, with the polar axis projected on the sky along a southeast/northwest direction. This disk is seen purely in silhouette, with no associated proplyd ionization front.

d216-0939 (Figure 1*g*). This giant silhouette disk and reflection nebula is located roughly 7' north-northwest of M43 in outer reaches of the Orion Nebula with very faint background nebular emission. This remarkable object is discussed in more detail in §4.

d253-1536 (Figure 1*h*). This large silhouette disk is unique in that it is apparently part of a binary system embedded within a giant proplyd in M43. This unusual disk and its associated proplyd and bipolar jet are discussed in detail in §5.

d280-1720 (Figure 1*i*). The southwestern part of M43 contains a star surrounded by a small disk seen in silhouette against the background nebular light. The disk has a major-axis diameter of roughly 0.8'' and a minor-axis diameter of about 0.6'' (370 \times 275 AU), implying that its polar axis is tilted about 45-50° out of the plane of the sky. The disk axis faces roughly toward P.A. \simeq 280°. However, the orientation and inclination can only be measured to about 10% accuracy due to the presence of the central star whose point spread function (PSF) makes the determination of the disk’s minor diameter difficult. This disk is seen purely in silhouette, with no associated proplyd ionization front.

d347-1535 (Figure 1*j*). This small disk is located about 1' north/northeast of NU Ori in M43. The disk is nearly edge-on, with an inclination of perhaps $\sim 80^\circ$. The disk diameter is roughly 0.7'' (320 AU) with the minor axis oriented along P.A. $\simeq 45^\circ = 225^\circ$. It has no identifiable central star, but does show clear evidence for a remarkable bipolar microjet or reflection nebula emerging perpendicular to the disk. Although the northeast part of the jet is brighter, the southwest portion intrudes farther into the disk perimeter, suggesting that this part of the jet or reflection nebula is tilted toward us. There is no proplyd ionization front that can be associated with this silhouette disk.

4. THE REFLECTION NEBULA OF d216-0939 AND THE HH 667 JET

This nearly edge-on disk is seen in silhouette against the very faint diffuse nebular light north of the Orion nebula and northwest of M43. A star and compact reflection nebula occupy the middle of the disk, while a more diffuse reflection nebula is illuminated primarily on its eastern face. A bipolar jet emerges orthogonal to the disk, and faint emission nebulae farther from the star constitute part of a larger bipolar flow, HH 667. This disk/jet system is discussed below.

4.1. Morphology of the Disk and Reflection Nebula

Figure 2 shows a more detailed view of d216-0939 than is given in Figure 1*g*. We deconvolved the original Cycle 11 images in each filter using 5 iterations of the LUCY task in IRAF,¹ with observations of a bright star about 5'' away adopted for the nominal PSF. With only 5 iterations, these deconvolved images did not yet have the signature artifacts from over-processing (rings were seen around stars after about 15 iterations), and the resulting effective FWHM spatial resolution we achieved was $\sim 0''.06$. In the 3-color image in Figure 2*a*, blue or white features are dominated by scattered starlight, while features that appear red/orange are dominated by H α and [N II] emission.

Even though this object is seen against the extremely faint outer parts of the Orion nebula, the *HST* image shows an unambiguous silhouette disk with a polar axis oriented at roughly $83^\circ=263^\circ$. The disk is shown best in the contour plot of H α in Figure 2*b*, where the blue-tinted contours trace extinction of background light. It is clear from this deconvolved image that the disk cuts all the way across the reflection nebula, indicating that the apparent bridge between the east and west sides in Figure 1*g* was caused by the PSF of *HST*. The deepest extinction in the disk reaches down to $\sim 20\text{--}30\%$ of the background nebula, corresponding to an optical depth of ~ 1.4 at 6563 Å and a grain column density of order 2×10^{-4} g cm $^{-2}$, with standard assumptions about the grain properties². Integrated over the surface of the disk, this would require a dust mass of order 1 M_\oplus , but of course this is only a lower limit since there could also be H α emission along our line of sight to the disk, or additional mass hidden in denser optically-thick and unresolved parts of the disk.

The diameter of the disk is at least 2''.6 (1200 AU), but could be somewhat larger if there is a more diffuse component at larger radii that is difficult to detect against the very faint nebular background. The clear extinction of background light by the outer edge of the silhouette disk gives a reliable estimate of the disk diameter, and means that it is not simply a shadow cast by a smaller disk, as in the bipolar reflection nebula around the young star ASR 41 in NGC 1333 (Hodapp et al. 2004). The gap between the east and west sides of the reflection nebula at 1''–1''.8 south of the central star may be this type of shadow, or it may indicate a larger diffuse disk not seen clearly in silhouette. This may be related to the fact that the silhouette disk appears somewhat asymmetric, having a size that is $\sim 50\%$ larger toward the north at the same contour level (Figure 2*b*). The silhouette is also curved slightly, with the concave opening toward the east, resulting from the contamination of reflected light.

The shape of the silhouette and the bright reflection nebula on its east-facing side indicate that the disk is flared (consistent with the expected appearance in 2-D models; Whitney & Hartmann 1992; Whitney et al. 2003a, 2003b), reaching latitudes of $\pm 13^\circ$ at its northern and southern extremities, where the projected width is about 0.6'' or 275 AU. Our line of sight to the central star is apparently very close to the flared surface of the disk, requiring that we view the system at a latitude comparable to the flare angle; thus, the disk axis is tilted by 10–15° out of the plane of the sky, with the eastern portion facing toward us. This viewing geometry and the resulting asymmetric nebula are reminiscent of the reflection nebula around VY CMa (Smith et al. 2001), except that the disk of VY CMa is not seen in silhouette. In the case of VY CMa, the star is apparently viewed along a line of sight close to the surface of the disk, and the position of the

¹IRAF is distributed by the National Optical Astronomy Observatories, which are operated by the Association of Universities for Research in Astronomy, Inc., under cooperative agreement with the National Science Foundation.

²Here we have assumed $Q_{\text{abs}}=0.08$ for $a=0.1$ μm grains at a wavelength of 6563 Å, and other typical grain properties to calculate the column mass (see Smith et al. 2004).

central star is wavelength dependent (Smith et al. 2001; Kastner & Weintraub 1998). However, in d216-0939, the central emission peak is the same in the F550M and F658N filters (Figure 2c), suggesting either that the star is viewed more directly, or that the dust grains in the protoplanetary disk are large and do not strongly redden the visual-wavelength light (see the discussion of the d114-426 disk by Shuping et al. 2003).

The d216-0939 disk and its reflection nebula closely resemble the well-studied HH 30 system in the L1551 dark cloud in Taurus (Burrows et al. 1996; Stapelfeldt et al. 1999), although the physical dimensions of this disk in Orion are several times larger than the HH 30 disk. This dark disk bisecting a bright reflection nebula is reminiscent of several other disks as well (e.g., Padgett et al. 1999; Stapelfeldt et al. 1998, 2003). The brightness contrast between the east and west halves in d216-0939 is stronger than in the two halves of HH 30; this is consistent with our conjectured inclination of the disk (with the axis tilted 10-15° from the plane of the sky), since Burrows et al. (1996) derive a slightly smaller tilt angle of $\sim 7.5^\circ$ (closer to edge-on) for HH 30. As discussed below, the similarity of d216-0939 and HH 30 is even further exemplified by their bipolar HH jets.

4.2. HH 667 – A Bipolar Jet From d216-0939

H α emission from HH 667 is presumably excited by shocks, but if it is instead an irradiated jet, the discussion below remains valid. This emission traces a bipolar outflow from the young star embedded in the d216-0939 disk. The ACS images reveal several knots near the central star, as well as more distant features about 30'' to the east and west.

HH 667 microjet: Figure 2 shows a system of emission knots along an axis perpendicular to the disk plane, within 1'' from the central peak. One bright elongated knot is seen $\sim 0.5''$ east of the star, and two fainter emission knots are seen west of the star along the outflow axis at $0.4''$ and $0.9''$ from the central peak. These are best seen in the contour map in Figure 2b and the intensity tracing in Figure 2c. These knots are seen in H α + [N II] $\lambda 6583$ line emission: they appear red/orange in the color image in Figure 2a, and the tracings in Figure 3c confirm that the H α emission from the knots has a clear excess compared to scattered continuum light in the F550M filter (whereas the central star in H α matches the continuum distribution).

This object is far from the center of M42 or M43, so if it is an irradiated jet or dominated by shock excitation, it is likely that the ionization fraction is low and that [N II] $\lambda 6583$ makes a significant contribution to the emission in the F658N filter. Therefore, we do not attempt to estimate the electron density from the H α emission measure here. High resolution spectra that could separate these two emission lines and measure kinematics would be useful for assessing the mass-loss rate in the HH 667 microjet.

HH 667 E: The eastern portion of this flow is marked by a partial bow shock located about 30'' from the source. This feature is several arcseconds in extent and consists of two sharp-edged filaments resembling bow shocks moving eastward (Fig. 3a). Very faint diffuse emission fills the interior of these bows on their western sides. The center of curvature of these partial bow shocks is $\sim 11^\circ$ off axis, suggesting that the flow may be bent toward the south.

HH 667 W: The western portion of the flow consists of several faint and diffuse filaments of emission elongated along the outflow axis, ranging from about 20'' to 30'' from the source (see Fig. 3). These features probably trace shocks within a faint jet. The components of HH 667 W are less than 1'' wide in the direction perpendicular to the flow axis, but unlike the eastern part of the flow, they are not significantly off-axis compared to the bipolar microjet and disk of the central star.

The maximum separation between the eastern and western components of the outflow from d216-0939 is $66''$ or about 0.15 pc in projection. Altogether, the d216-0939 disk and its more extended HH 667 outflow closely resemble the well-studied HH 30 system in the L1551 dark cloud in Taurus (Burrows et al. 1996; Stapelfeldt et al. 1999).

5. d253-1536 AND THE HH 668 JET

Ground-based narrowband images of the H II region M43 revealed a compact globule with a central star embedded within the western rim of this nebula. The ACS images (Figure 4) show that the object is in fact a proplyd ionization front or shock surrounding two stars separated by $1''.1$: the brighter star is visible on ground-based images, and near it is a fainter star embedded in a silhouette disk. The second object, d253-1536, drives a microjet visible on one side of the disk, and the larger bipolar HH 668 jet that breaks-out on both sides of the proplyd’s bright rim in a direction perpendicular to the disk. A bow shock (HH 668 A) is seen almost $1'$ away from the central star to the south/southeast. The various components of d253-1536 and the HH 668 jet are summarized in Figure 4 and are discussed below.

5.1. The d253-1536 Disk and Bright Rim

A $0''.6 \times 1''.4$ disk seen in silhouette against background nebular emission of M43 is located $1''.1$ due east of the brighter star. Assuming that the d253-1536 disk is circular, the axis of the disk is inclined by $\sim 25^\circ$ with respect to the plane of the sky. However, the disk has pronounced asymmetry. The brightest pixel, presumably produced by a compact reflection nebula located somewhat south of the star’s true location, is displaced from the disk center by about $0''.15 - 0''.2$ toward the east. This distortion provides evidence that the bright star and the disk form a true physical pair in which the gravitational perturbations of the brighter and presumably more massive star generate the disk asymmetry. The d253-1536 disk is remarkable for being the secondary member of a binary system in which the primary is a brighter star that shows no indication of being surrounded by a visible disk. The secondary is decentered in its own circumstellar disk, but powers a remarkably straight bipolar jet (see below), suggesting that the orbital period is much longer than the flow timescale in the visible jet. Thus, the orbital timescale must be >100 yr. For the apparent separation of $1''.1$ or $a \simeq 250$ AU, we find that the orbital period would be $\sim 4,000 (M/M_\odot)^{-0.5}$ yr, where M is the total mass of the binary system. These are not tight constraints on the system’s parameters, but at least they are consistent. There is no evidence for a larger circumbinary disk around the system.

Both members of this binary system are embedded within a proplyd ionization front that faces directly toward NU Orionis, the early B-type exciting star of the M 43 H II region. The bright rim’s radius is about $3''$ (1400 AU), so the diameter of this object is comparable to some of the giant proplyd candidates seen recently in the Carina nebula (Smith et al. 2003). The ionization front is highly structured and consists of a series of scalloped rims, perhaps signifying instabilities in a shock front rather than a smooth ionization front. An anonymous referee pointed out that this feature bears a remarkable resemblance to the bright cusp seen around the dark proplyd d114-426 (O’Dell & Beckwith 1997).

5.2. The HH 668 Jet

A faint microjet (see §5.3) emerges from the center of the disk on its south side, and its faint emission can be traced to the edge of the proplyd’s bright rim about $4''$ to the south (Fig. 4*b*). Then, as it breaks out of the proplyd ionization front, the jet becomes brighter (HH 668 S) and can be traced for another $8''$ toward the south along the same axis, which is perpendicular to the silhouette disk. Although the jet blends into the background nebular light of M43 at this point, the flow continues farther to the south, since a bright bow shock is located $55''$ south on the jet axis (HH 668 A in Figs. 4*a*, *c*, and *d*). This south-facing bow shock has a compact $0''.5 - 1''$ -diameter apex located at $\alpha(2000) = 5^h 35^m 26.^s6$, $\delta(2000) = -5^\circ 16' 25''$, with an extended wing of H α emission that trails back toward the source along its western rim for about $10''$ (Figs. 4*a* and *c*). This feature is probably the trailing edge of the bow shock. HH 668 A has a width of only several tenths of an arcsecond and has been missed on ground-based images. The head of the bow shock is also bright in [O III] (Fig. 4*d*), indicating shock speeds of $\sim 100 \text{ km s}^{-1}$.

A counter-jet (HH 668 N) emerges from the northern side of the object and can be traced out to at least $10''$ from the center of the silhouette disk (Fig. 4*b*). Thus, the bipolar HH 668 jet from the disk in this binary star system has a projected spatial extent of at least $65''$ (0.14 pc), similar to HH 667. A line connecting HH 668 N and S passes directly through the center of the d253-1536 disk, and comes within a few degrees of the HH 668 A bow shock. Thus, we do not detect major deflection of the jet by a large scale wind in M43 or precession of the jet due to orbital motion in the binary system, as mentioned above in §5.1. However, proper motions do reveal some deviations from a purely linear jet (see §5.4). The N and S components of the HH 668 jet (Fig. 4*b*) are brightest immediately outside the proplyd’s bright cusp, implying that at least in this portion of the flow, HH 668 is an irradiated jet.

5.3. The HH 668 Microjet From d253-1536

Figure 5 shows details of the HH 668 microjet emerging from d253-1536. Like most of the nearly two dozen microjets from proplyds in Orion (Bally et al. 2000), it appears to be a one-sided jet where the counter-jet is faint and lost in the bright background nebular light. The jet is brightest on the southeast side of the disk, which may be more directly illuminated by NU Ori in the center of M43.

We obtained F658N images of d253-1536 during both Cycles 11 and 12 (2002 August and 2004 January, respectively), allowing us to document temporal changes in the microjet structure. Clear qualitative differences are seen in Figures 5*a* and 5*b*: in 2002 August (Fig. 5*a*) the HH 668 microjet shows one bright emission knot located roughly $0''.2$ left of the star (note that the images in Fig. 5 are rotated so that the horizontal direction is along P.A.= 170°), while 513 days later in 2004 January (Fig. 5*b*) two distinct knots are seen. If we assume that the second knot farther from the star in 2004 January is the same condensation as the single knot seen in 2002 August, then the centroid of this condensation has moved $0''.195$, indicating a transverse velocity in the plane of the sky of roughly 300 km s^{-1} . With the d253-1536 disk axis tilted $\sim 25^\circ$ from the plane of the sky (see §5.1), the true speed of the HH 668 microjet is roughly 330 km s^{-1} . This is on the high end compared to typical microjet speeds, and is significantly faster than downstream portions of the HH 668 jet (see Table 3 and §5.4), implying that the flow decelerates when it interacts with the ambient medium or downstream jet material, as expected in conventional HH flows.

The observed H α surface brightness can be used to estimate the electron density of the knots in the HH 668 microjet, with the important caveats that this will be an underestimate if the jet is not fully ionized

and an overestimate if there is significant contamination by [N II] $\lambda 6583$ in the filter.³ The electron density is given by

$$n_e = \sqrt{\frac{EM}{L_{\text{pc}}}}$$

where $EM = 4.89 \times 10^{17} I(H\alpha)$ is the emission measure in $\text{cm}^{-6} \text{pc}$ (Spitzer 1978), and $I(H\alpha)$ is the observed $H\alpha$ surface brightness in $\text{ergs s}^{-1} \text{cm}^{-2} \text{arcsec}^{-2}$. L_{pc} is the typical emitting path length or the diameter of the jet in pc. From the tracings in Figure 5c we see that a typical value for $F_\lambda(H\alpha)$ in the knots is $\sim 2 \times 10^{-16} \text{ergs s}^{-1} \text{cm}^{-2} \text{\AA}^{-1} \text{arcsec}^{-2}$, or $I(H\alpha) \simeq 8 \times 10^{-16} \text{ergs s}^{-1} \text{cm}^{-2} \text{arcsec}^{-2}$ integrated over the 37.2\AA effective width of the F658N filter. Adopting a jet width of $\sim 0''.1$ or $L = 46 \text{ AU}$ as seen in images, we find $n_e \gtrsim 4 \times 10^3 \text{ cm}^{-3}$. (Again, this is probably a lower limit, since the calculation does not include a correction for the ionization fraction and because the jet width may be unresolved.)

Combining this electron density with the speed measured in proper motions can yield an estimate of the mass-loss rate of the microjet very close to the point of origin. To do this, we must consider that the observed emission knots may be either discrete blobs of gas, or may be shocks in an otherwise steady flow. In the first case, we must average the electron density over the distance between the knots, so likely values for the jet density are in the range $1\text{--}4 \times 10^3 \text{ cm}^{-3}$ (i.e., adopting an appropriate pseudo filling-factor). The average mass-loss rate is given by

$$\dot{M} = \pi \left(\frac{L}{2}\right)^2 m_H n_e v$$

yielding $\dot{M} \gtrsim 3 \times 10^{-10} (n_e/10^3) M_\odot \text{ yr}^{-1}$. Since $n_e = 4 \times 10^3 \text{ cm}^{-3}$ is an underestimate for the reasons stated above, the likely current mass loss rate in the HH 668 microjet is of order $10^{-9} M_\odot \text{ yr}^{-1}$.

5.4. Proper Motion of HH 668

As noted above, we obtained *HST*/ACS F658N images of d253-1536 and HH 668 in both Cycle 11 and Cycle 12, allowing us to search for proper motion in the components of the HH 668 jet using the “difference-squared” method (e.g. Bally et al. 2002; Hartigan et al. 2001) optimized for the measurement of nebular proper motions. The two sets of images were obtained 513 days (1.4 years) apart. At a distance of 460 pc assumed for this portion of the Orion nebula, a one pixel ($0''.05$) shift in this time interval corresponds to a velocity of about 75 km s^{-1} . On bright and compact features, our image comparison method can determine motions to an accuracy of about 0.1 to 0.3 pixels, or about 10 to 20 km s^{-1} . The resulting proper motions for components of the HH 668 jet are listed in Table 3.⁴ Figure 6 is similar to Figure 4, except that the proper motions of various knots measured by this method are over-plotted and subcomponents of the jet are labeled, corresponding to the names in Table 3. In Figure 6a, the arrows show the amount of motion

³We made no attempt to correct for the uncertain contribution of [N II] $\lambda 6583$, as the required information is not yet available. To flux calibrate the images, we simply followed the standard calibration method for *HST* imaging data – i.e., using the PHOTFLAM and PHOTBW values.

⁴The bottom row of Table 3 lists the results of measuring proper motion of a reference star, giving the method’s measurement uncertainty.

extrapolated to 50 years, while in the close-up view in Figure 6*b*, the arrows correspond to motion in 20 years.

The bipolar jet emerging from the silhouette disk exhibits motions with velocities that decline from around 300 km s^{-1} for the microjet within $1''$ of the central star (see above) to about 215 km s^{-1} at a distance $10''$ south. A similar decline of more than 30% in the jet speed is seen toward the north.

The HH 668 flow can be traced about $50''$ south to a prominent $\text{H}\alpha$ bow shock (HH 668A). Faint wings of $\text{H}\alpha$ emission sweep back along the western rim of this feature toward the source for more than $15''$. A compact high-excitation region bright in $[\text{O III}] \lambda 5007$ lies about an arcsecond upstream from the tip of the shock. The proper motion of the HH 668 A shock in $\text{H}\alpha$ is about 140 km s^{-1} toward the southeast; this speed is sufficient to account for the excitation of the $[\text{O III}] \lambda 5007$ emission line seen there. Since HH 668 A is the only part of the flow showing detectable $[\text{O III}]$ emission, this is probably the terminal bow shock. A fainter sub-arcsecond diameter knot of high proper motion material is located between the source and this bow shock about $40''$ south from the source (HH 668 B; see Fig. 6*a*). This knot shows proper motions of about 110 km s^{-1} along the HH 668 flow axis, but has no $[\text{O III}]$ emission, so it is an internal working surface of the jet. A few other knots were seen upon blinking images at the two epochs, but these did not yield statistically significant results with our proper motion measurement technique. HH 668 A and B located relatively far from the source support a general trend of a systematic decline in the proper motions with increasing distance from the source.

The proper motion vectors show evidence for a systematic deflection of the HH 668 bipolar outflow toward the east by about 10° . This mild deflection is unusual in that it is toward the source of ionizing radiation NU Ori. A possible explanation for this behavior is that the motion of plasma within this portion of the M 43 H II region is dominated by the flow of material away from the western ionization front located just beyond the right edge of Figure 4.

6. CONCLUSIONS

Our *HST*/ACS imaging survey of the outer parts of Orion and M43 yielded the discovery of 9 new disks seen in silhouette against faint background light, and they show important new details for one previously discovered silhouette disk. Compared to other silhouette disks, several members of this new sample are unusual in that they show evidence for bipolar reflection nebulae or microjets. This may be a selection effect due to the fainter background levels far from the Trapezium. Two of the new disks in our sample are found in or near M43 and deserve special attention:

1. d216-0939 is a nearly edge-on disk with a remarkable reflection nebula and a bipolar microjet that resembles the HH 30 disk/jet system in Taurus. The disk is as large as the largest previously-known silhouette disk. It also drives the 0.15 pc long bipolar jet HH 667.

2. d253-1536 is also a very large silhouette disk, and is the only silhouette disk known so far to exhibit tidal distortions induced by a companion star in a binary system. It is located inside the M43 H II region, and is associated with a bright proplyd ionization front. The disk drives both a microjet and a larger 0.14 pc long bipolar jet called HH 668. Images taken during Cycles 11 and 12 reveal detectable proper motions in the jet, with de-projected speeds as high as 330 km s^{-1} . With an electron density of order $4 \times 10^3 \text{ cm}^{-3}$ near the source, this implies a mass-loss rate of roughly $10^{-9} M_\odot \text{ yr}^{-1}$.

We thank an anonymous referee for a timely and helpful review. HH catalog numbers are assigned by B. Reipurth in order to correspond with the list of Herbig-Haro objects that he maintains (see <http://ifa.hawaii.edu/reipurth/>). Support was provided by NASA through grants GO-9460, GO-9825, and HF-01166.01A from the Space Telescope Science Institute, which is operated by the Association of Universities for Research in Astronomy, Inc., under NASA contract NAS5-26555.

REFERENCES

- Bally, J., Heathcote, S., Reipurth, B., Morse, J.A., Hartigan, P., & Schwarz, R. 2002, *AJ*, 123, 2627
- Bally, J., Licht, D., Smith, N., & Walawender, J. 2004, *AJ*, in press
- Bally, J., O'Dell, C. R., & McCaughrean, M. 2000, *AJ*, 119, 2919
- Bally, J., & Reipurth, B. 2001, *ApJ*, 546, 299
- Bally, J., Sutherland, R. S., Devine, D., & Johnstone, D. 1998, *AJ*, 116, 293
- Burrows, C.J., et al. 1996, *ApJ*, 473, 437
- Chen, H., et al. 1998, *ApJ*, 492, L173
- Hartigan, P., Morse, J.A., Reipurth, B., Heathcote, S., & Bally, J. 2001, *ApJ*, 559, L157
- Hodapp, K.W., Walker, C.H., Reipurth, B., Wood, K., Bally, J., Whitney, B.A., & Connelley, M. 2004, *ApJ*, 601, L79
- Kastner, J.H., & Weintraub, D.A. 1998, *AJ*, 115, 1592
- McCaughrean, M.J., & O'Dell, C.R. 1996, *AJ*, 111, 1977
- McCaughrean, M.J., et al. 1998, *ApJ*, 492, L157
- McCullough, P.R., et al. 1995, *ApJ*, 438, 394
- O'Dell, C.R., & Beckwith, S. 1997 *Science*, 276, 1355
- O'Dell, C.R., & Wong, S.-K. 1996, *AJ*, 111, 846
- O'Dell, C. R., Wen, Z., & Hu, X. 1993, *ApJ*, 410, 696
- O'Dell, C.R. 2001, *AJ*, 122, 2662
- Padgett, D.L., Brandner, W., Stapelfeldt, K.R., Strom, S.E., Terebey, S., & Koerner, D. 1999, *AJ*, 117, 1490
- Reipurth, B., & Bally, J. 2001, *ARAA*, 39, 403
- Shuping, R.Y., Bally, J., Morris, M., & Throop, H. 2003, *ApJ*, 587, L109
- Smith, N., Bally, J., & Morse, J.A. 2003, *ApJ*, 587, L105
- Smith, N., Barbá, R.H., & Walborn, N.R. 2004, *MNRAS*, 351, 1457
- Smith, N., Humphreys, R.M., Davidson, K., Gehrz, R.D., Schuster, M.T., & Krautter, J. 2001, *AJ*, 121, 1111
- Spitzer, L. 1978, *Physical Processes in the Interstellar Medium* (New York: Wiley)
- Stapelfeldt, K.R., et al. 1999, *ApJ*, 516, L95
- Stapelfeldt, K.R., Krist, J.E., Menard, F., Bouvier, J., Padgett, D.L., & Burrows, C.J. 1998, *ApJ*, 502, L65
- Stapelfeldt, K.R., Menard, F., Watson, A.M., Krist, J.E., Dougados, C., Padgett, D.L., & Brandner, W. 2003, *ApJ*, 589, 410
- Störzer, H., & Hollenbach, D. 1998, *ApJ*, 502, L71
- Whitney, B.A., & Hartmann, L. 1992, *ApJ*, 395, 529
- Whitney, B.A., Wood, K., Bjorkman, J.E., & Cohen, M. 2003a, *ApJ*, 598, 1079
- Whitney, B.A., Wood, K., Bjorkman, J.E., & Wolff, M.J. 2003b, *ApJ*, 591, 1049

Table 1. Cycle 11 ACS/WFC Observations

Object	α_{2000}	δ_{2000}	Filter	Exposure (sec)
M43-NW	5 35 22.6	-5 16 09	F658N	2 × 500
M43-NW	5 35 22.6	-5 16 09	F660N	2 × 500
M43-NW	5 35 22.6	-5 16 09	F550M	30
M43-NW	5 35 22.6	-5 16 09	F502N	4 × 500
M42 North	5 35 20.5	-5 11 17	F658N	2 × 500
M42 North	5 35 20.5	-5 11 17	F660N	2 × 500
M42 North	5 35 20.5	-5 11 17	F550M	30
M42 North	5 35 20.5	-5 11 17	F502N	4 × 500

Table 2. New Silhouette Disks in Orion and M43

Object	α_{2000}	δ_{2000}	Diameter	Comments
d053-717	5 35 05.41	-5 27 17.2	0''9	small disk, bright star
d110-3035	5 35 10.99	-5 30 35.2	0''9	bipolar jet/refl. neb.
d124-132	5 35 12.38	-5 21 31.5	0''5	proplyd, jet?
d132-042	5 35 13.24	-5 20 41.9	0''5	proplyd, jet
d132-1832	5 35 13.24	-5 18 33.0	1''0	variable star, swept disk
d141-1952	5 35 14.05	-5 19 52.1	0''7	small disk, bright star
d216-0939	5 35 21.57	-5 09 38.9	2''6	giant, edge-on, refl. neb., HH 667
d253-1536	5 35 25.30	-5 15 35.5	1''5	giant proplyd, binary, sil. disk, HH 668
d280-1720	5 35 28.04	-5 17 20.2	0''8	small disk, bright star
d347-1535	5 35 34.67	-5 15 34.8	0''7	bipolar jet/refl. neb.

Table 3. Proper Motions of the HH 668 Jet

Name	$\alpha(J2000)$ h m s	$\delta(J2000)$ ° ' ''	X ('')	Y ('')	D ('')	V (km s ⁻¹)	PA (V) (°)	PA (S) (°)	age (years)
N3	5 35 25.01	-5 15 24.4	-4.3	11.1	11.9	84.5±21.8	354.1	338.8	307
N2	5 35 25.08	-5 15 26.0	-3.3	9.4	10.0	275.1±8.4	340.3	340.8	79
N1	5 35 25.14	-5 15 28.8	-2.4	6.7	7.1	275.1±8.4	340.3	340.5	55
microjet	5 35 25.31	-5 15 35.9	0.09	-0.49	0.5	303.5±8.0	170.0	170.0	3.6
S1	5 35 25.39	-5 15 39.9	1.4	-4.4	4.6	245.6±6.0	160.2	162.9	40
S2	5 35 25.43	-5 15 41.5	2.0	-6.0	6.3	108.8±16.0	145.3	161.6	126
S3	5 35 25.48	-5 15 42.7	2.7	-7.2	7.7	178.2±16.0	159.7	159.9	94
B	5 35 26.08	-5 16 10.4	11.7	-34.9	36.8	111.8±14.0	160.4	161.4	717
A	5 35 26.61	-5 16 25.2	19.6	-49.7	53.4	143.3±8.4	154.3	158.5	812
ref. star	5 35 27.06	-5 15 44.6	26.2	-9.2	27.8	5.9±6.0	...	109.2	...

Note. — Column 1: Name of each knot (see Figure 6). Column 2 & 3: The J2000 coordinates of each box center.: Column 4: The projected distance from d253-1536 along the R.A. direction in arc seconds. Column 5: The projected distance from d253-1536 along the DEC direction in arc seconds. Column 6: The projected distance from d253-1536 along the jet axis in arc seconds. Column 7: The proper motion in km s⁻¹. Column 8: The position angle of the measured velocity vector. Column 9: The position angle of a line drawn from d253-1536 to the center of the box. Column 10: The dynamical age of the feature (D/V) assuming a distance of 460 pc (the microjet age corresponds to the Cycle 12 observation).

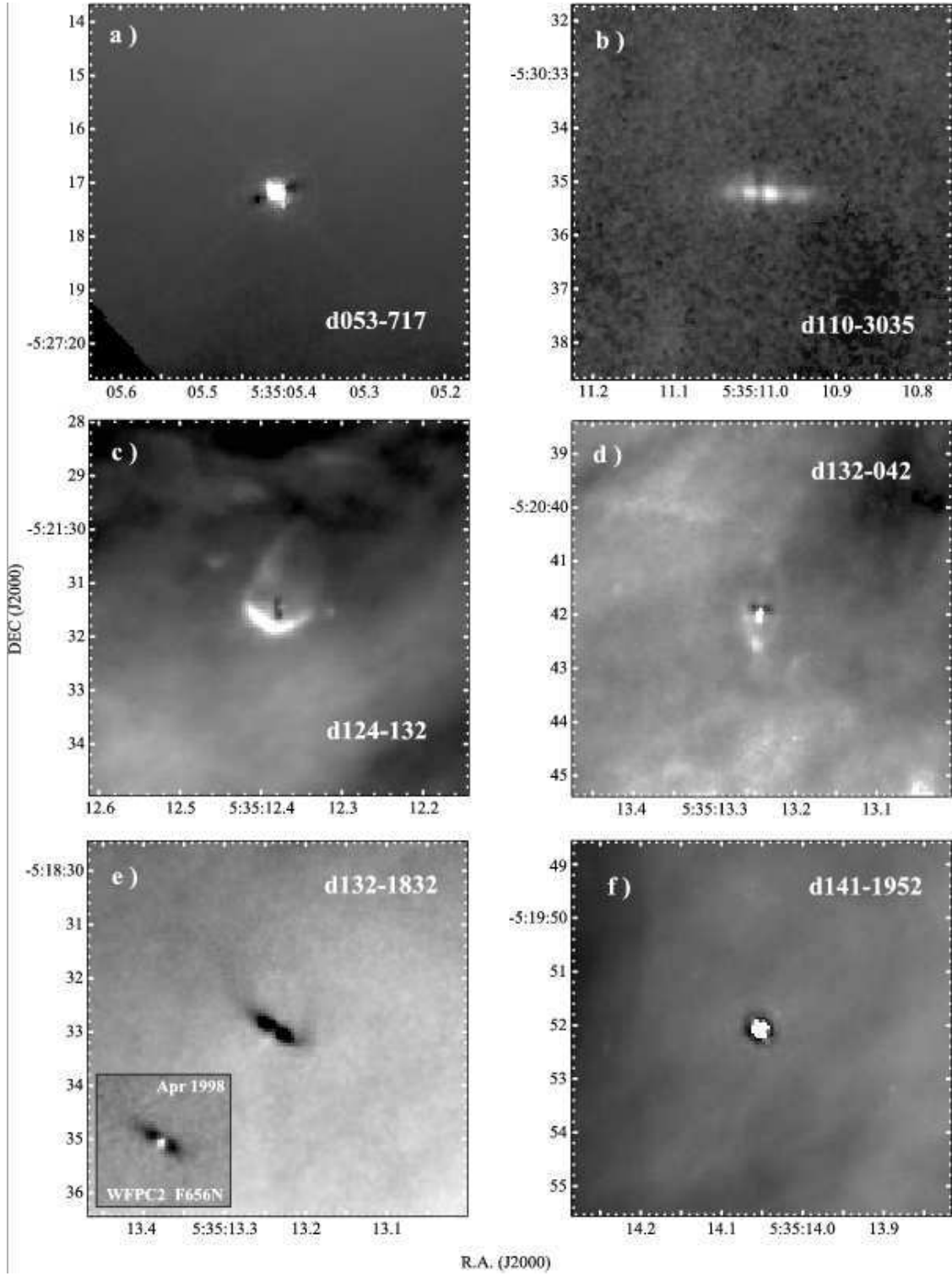


Fig. 1.— ACS/WFC F658N ($H\alpha$) images of selected silhouette disks in the outskirts of the Orion Nebula and M43. All are newly-discovered disks, except d132-1832 in panel (e), shown here because of new structures seen in the outer parts of the disk and because of the variable central star (inset; see text).

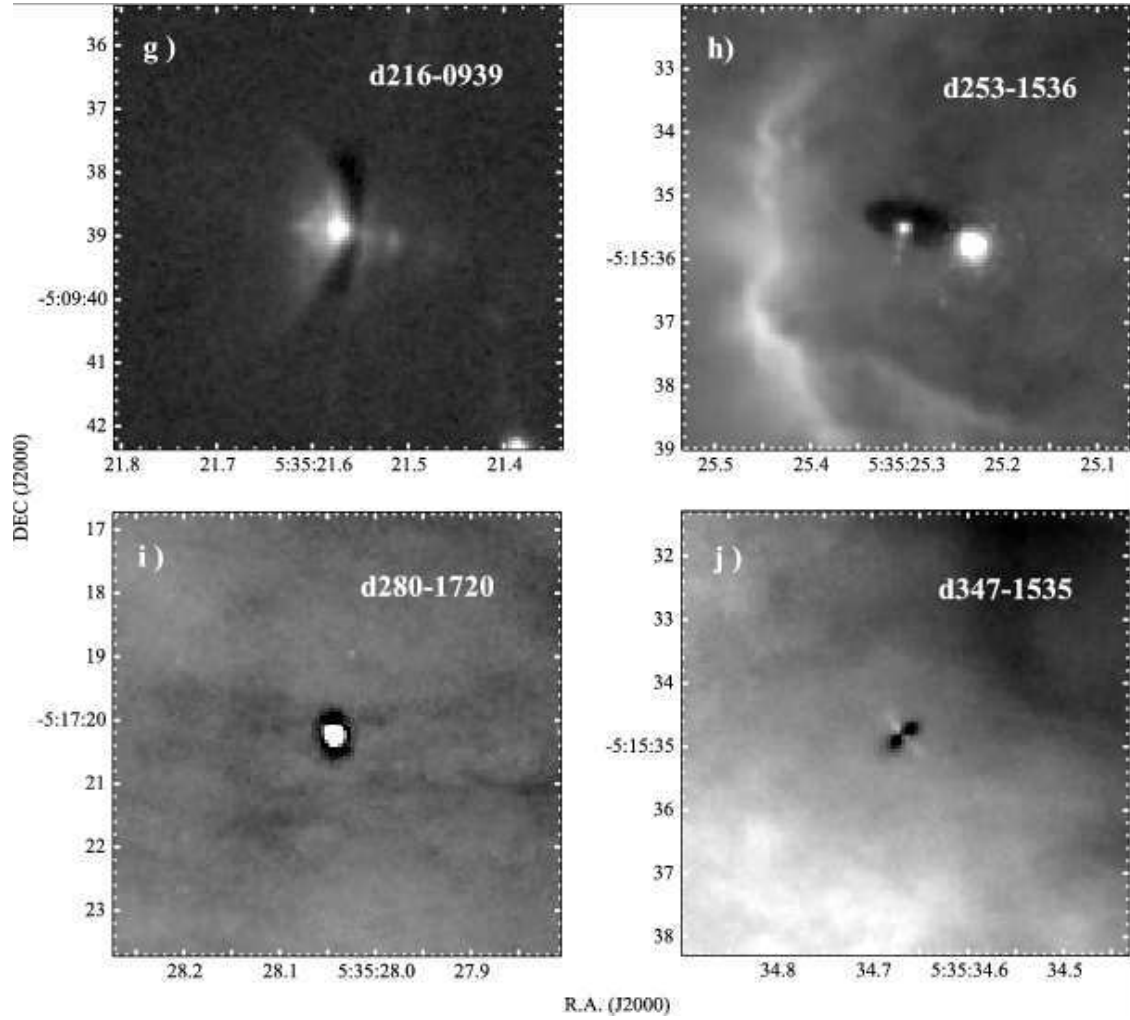


Fig. 1.— continued.

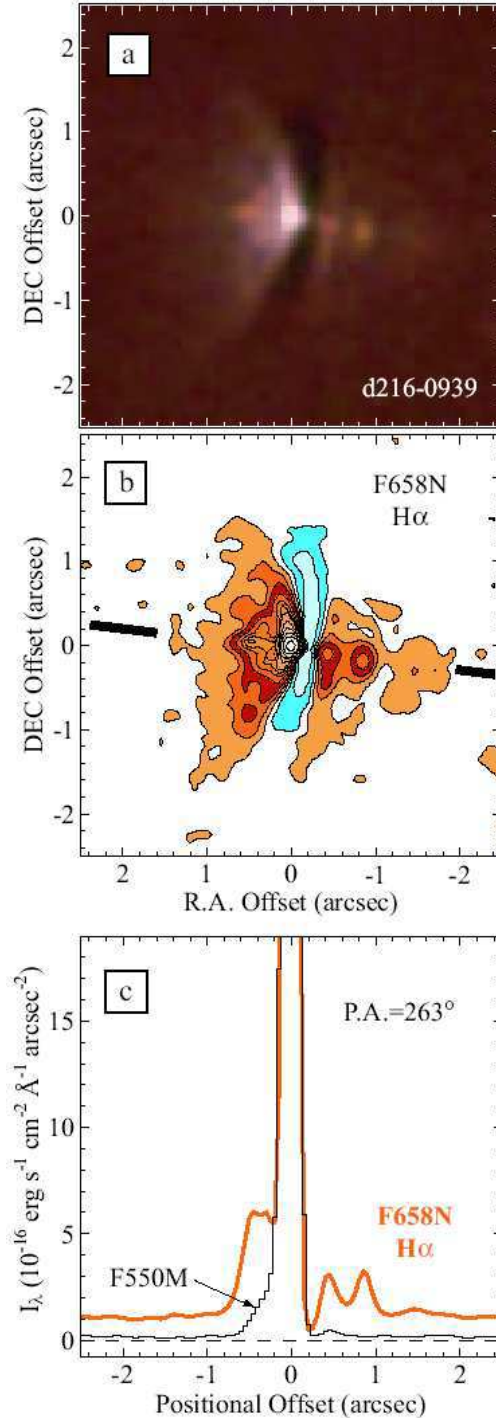


Fig. 2.— (a) 3-color image of the reflection nebula d216-0939, with F550M in blue, F660N in green, and F658N in red. (b) Contour plot of the deconvolved F658N H α image of d216-0939. The two lowest contours are blue and signify extinction of the background nebular light, and are drawn at 0.5 and $0.7 \times 10^{-16} \text{ erg s}^{-1} \text{ cm}^{-2} \text{ \AA}^{-1} \text{ arcsec}^{-2}$. The remaining contours are orange and are emission above the background. The lowest contour is roughly 3σ above the background, and is drawn at $0.95 \times 10^{-16} \text{ erg s}^{-1} \text{ cm}^{-2} \text{ \AA}^{-1} \text{ arcsec}^{-2}$. The remaining contours are drawn at $1.2, 1.6, 2.5, 3.7, 4.8, 6, 10, 20, 40, 80,$ and $200 \times 10^{-16} \text{ erg s}^{-1} \text{ cm}^{-2} \text{ \AA}^{-1} \text{ arcsec}^{-2}$. (c) Intensity tracings along P.A.= 263° through the central peak (marked by the black lines in the middle panel) for the F658N (thick orange line) and F550M (black histogram) filters.

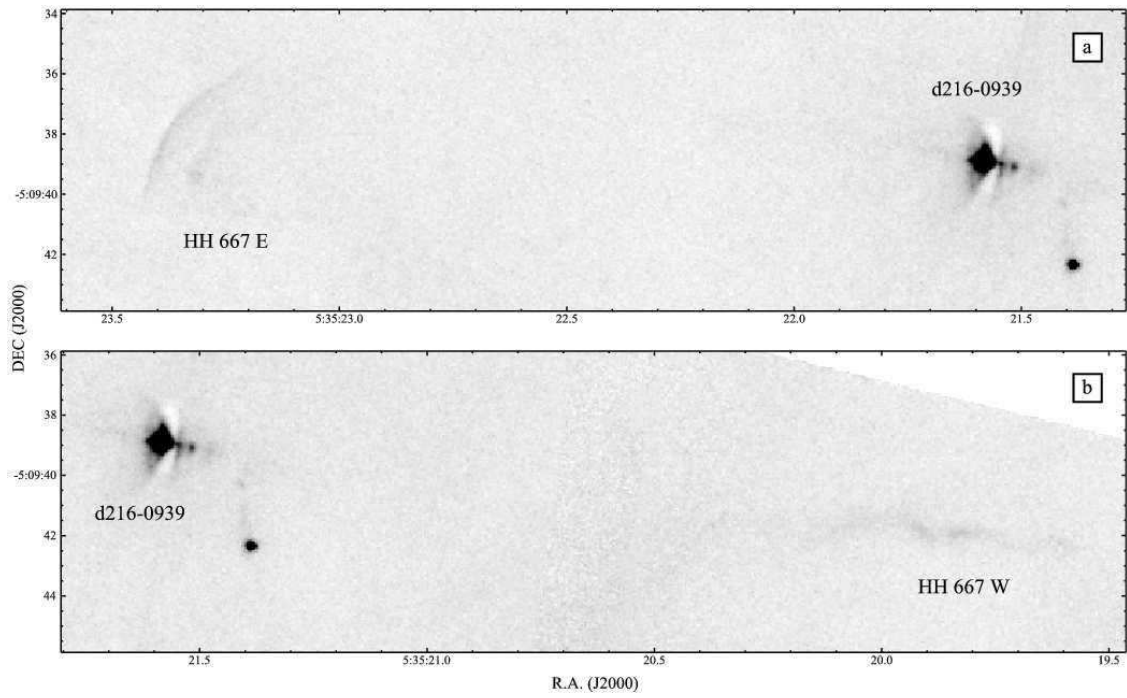


Fig. 3.— HH 667, candidate bow shocks in the jet from d216-0939. These images are displayed in negative grayscale. (a) the eastern portion of the jet, with a curved bow shock (HH 667 E). (b) the western portion of the jet, with emission filaments along the jet axis (HH 667 W).

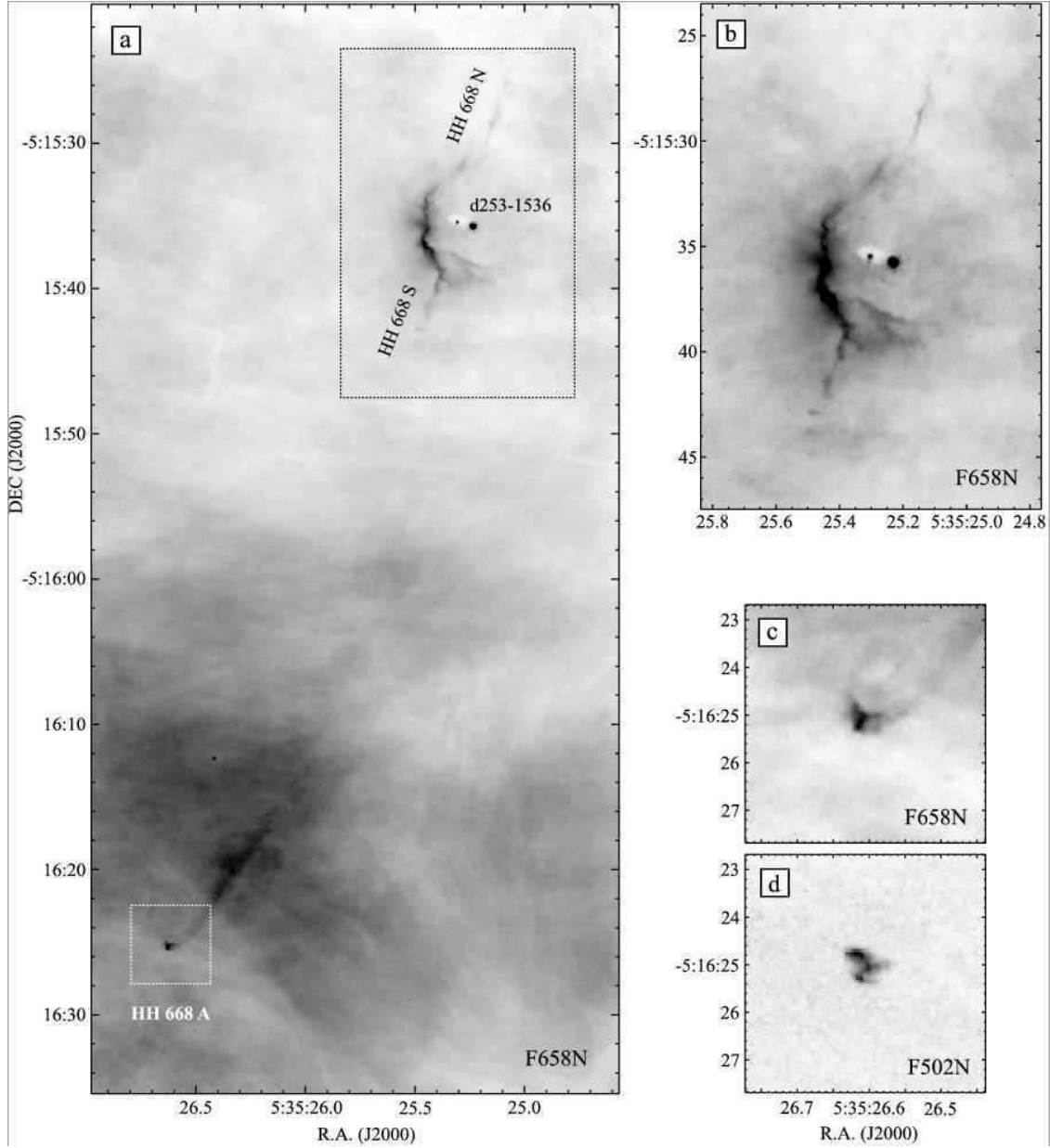


Fig. 4.— Images of the binary protoplanetary disk d253-1536 and the HH 668 jet with negative grayscale display. (a) Large scale image showing the alignment of the bipolar jet from d253-1536, which is perpendicular to the disk, and the bow shock HH 668 A. (b) detail of the d253-1536 protoplanetary disk and the HH 668 jet. (c) and (d) are details of the HH 668 A bow shock in $H\alpha$ (F658N) and $[O\ III]\ \lambda 5007$ (F502N) emission, corresponding to the small white box in Panel a.

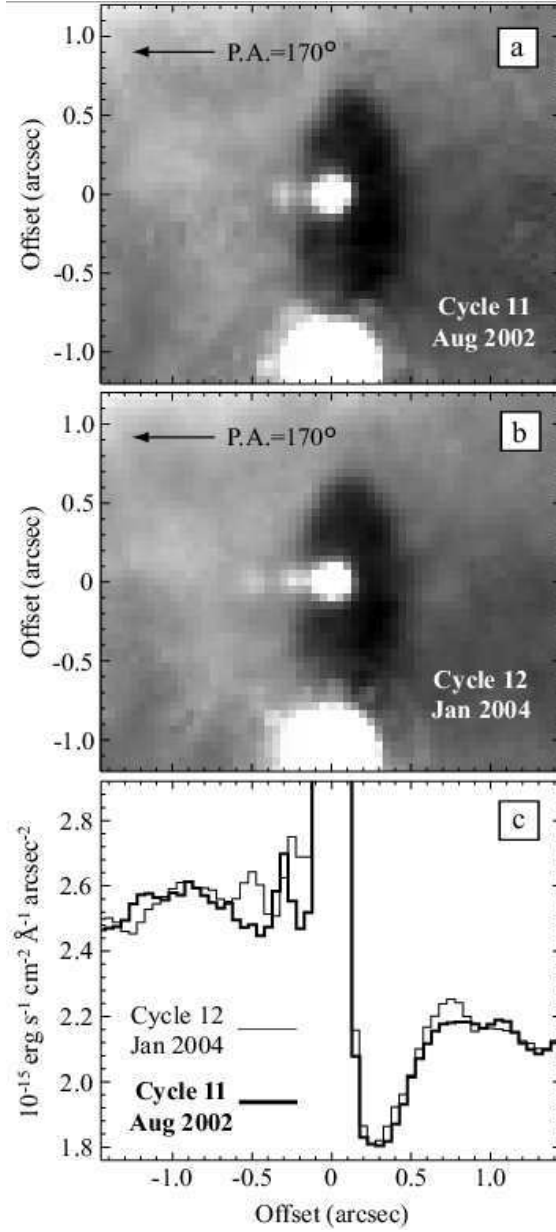


Fig. 5.— The HH 668 microjet of d253-1536 at two epochs. (a) Cycle 11 F658N image obtained in August 2002, rotated so that P.A.=170° is to the left. (b) same as Panel *a* but for Cycle 12 obtained in January 2004. (c) Intensity tracings of H α (F658N) emission for both Cycles 11 and 12, passing through the star at P.A.=170°=350°, showing the motion of the knots to the left of the star in Panels *a* and *b*. A new knot has appeared in Cycle 12, while the bright knot seen in Cycle 11 has moved. Cycle 11 is the thicker line, and Cycle 12 is the thinner line.

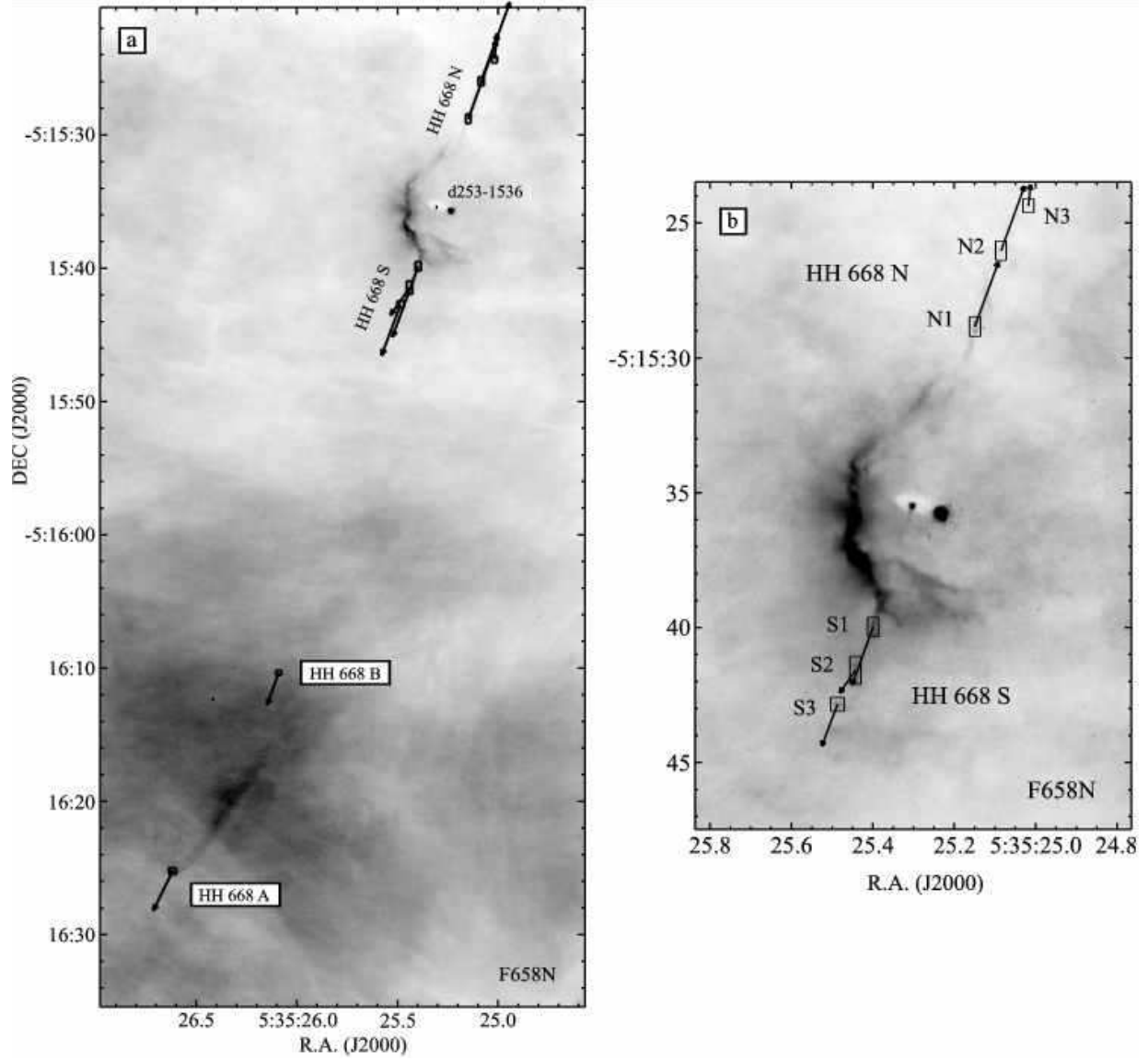


Fig. 6.— Same as for Figure 4, but showing proper motion vectors for various features as described in the text and listed in Table 3. Panel (a) shows an expanded view of the HH 668 jet, with the vectors corresponding to extrapolated motion in 50 yr, while panel (b) shows a zoomed-in view of HH 668 N and S, where the vectors correspond to extrapolated motion in 20 yr.